Mathematical Medicine and Biology (2017) **00**, 1–24
doi: 10.1093/imammb/dqw022

A discrete in continuous mathematical model of cardiac progenitor cells formation and growth as spheroid clusters (Cardiospheres)

EZIO DI COSTANZO
Istituto per le Applicazioni del Calcolo – Consiglio Nazionale delle Ricerche, Via dei Taurini 19 – 00185 Rome, Italy

ALESSANDRO GIACOMELLO
Department of Molecular Medicine, Pasteur Institute Cenci–Bolognetti Foundation, Sapienza University of Rome, Viale del Policlinico – 00161 Rome, Italy

ELISA MESSINA
Department of Pediatric Cardiology, Sapienza University of Rome, Viale Regina Elena 324, 00161, Rome, Italy

ROBERTO NATALINI* AND GIUSEPPE PONTRELLI
Istituto per le Applicazioni del Calcolo – Consiglio Nazionale delle Ricerche, Via dei Taurini 19 – 00185 Rome, Italy
*Corresponding author: Email: roberto.natalini@cnr.it

FABRIZIO ROSSI
Department of Molecular Medicine, Pasteur Institute Cenci–Bolognetti Foundation, Sapienza University of Rome, Viale del Policlinico – 00161 Rome, Italy

ROBERT SMITS
Department of Mathematical Sciences, New Mexico State University, Las Cruces, NM 88003, USA

AND

MONIKA TWAROGOWSKA
Istituto per le Applicazioni del Calcolo – Consiglio Nazionale delle Ricerche, Via dei Taurini 19 – 00185 Rome, Italy

[Received on 22 December 2015; revised on 8 November 2016; accepted on 28 November 2016]

We propose a *discrete in continuous* mathematical model describing the in vitro growth process of biophsy-derived mammalian cardiac progenitor cells growing as clusters in the form of spheres (*Cardiospheres*). The approach is hybrid: discrete at cellular scale and continuous at molecular level. In the present model, cells are subject to the self-organizing collective dynamics mechanism and, additionally, they can proliferate and differentiate, also depending on *stochastic processes*. The two latter processes are triggered and regulated by chemical signals present in the environment. Numerical simulations show the structure and the development of the clustered progenitors and are in a good agreement with the results obtained from in vitro experiments.

Keywords: mathematical biology; differential equations; hybrid models; Poisson stochastic process; collective dynamics; cell movements; cellular signalling; chemotaxis; stem cells; Cardiospheres.

1. Introduction

First described in 2004, the cardiac biopsy-derived progenitor cells, growing in vitro as 'niche'-like micro-tissue, known as *Cardiospheres* (CSps), represent a widely adopted platform technology holding great promise to realize a powerful cell therapy system, in vitro drug screening and disease modelling opening new opportunities for myocardial repair (Messina *et al.*, 2004; Ruckdeschel *et al.*, 2007; Li *et al.*, 2010). To achieve this goal, an optimal management of qualitative and quantitative CSps growth-modifying factors in terms of cell proliferation, differentiation and interaction with the external environment has to be known. It requires a simulator of the features and the fate of the CSps-niche-system which is based on new as well as already existing experimental biological data and on reliable mathematical models.

Our aim is to model the formation and differentiation of the original 3D cardiac biopsy-derived heart progenitors in vitro system, that is the CSp. These structures are cellular spheroids with a central nucleus of less differentiated elements surrounded by outer layers of cells more committed toward different levels of cardio-vascular differentiation with other proliferation features (Fig. 1a). Their individual formation in vitro starts from a few (low differentiated and less specialized) progenitor cells which are cultured in a carefully chosen environment and under specific conditions (Messina *et al.*, 2004; Chimenti *et al.*, 2012), and have the potential to develop into a more cardiac-specific differentiation which, unless derived from pre-natal hearts, are no longer able to achieve a terminal level of contractile cardiomyocytes. The major types of molecular processes that control cellular differentiation and proliferation involve various physical factors, nutrients and cell signaling. During the multiple stages of development, the cell size and shape changes dramatically, as a response to signalling molecules (Brown *et al.*, 2003; Agathocleous & Harris, 2013). This biological environment is similar to that of tumour spheroids as described in Wallace & Guo (2013). Neoplastic cells hold several growth strategies, such as genetic mutation of

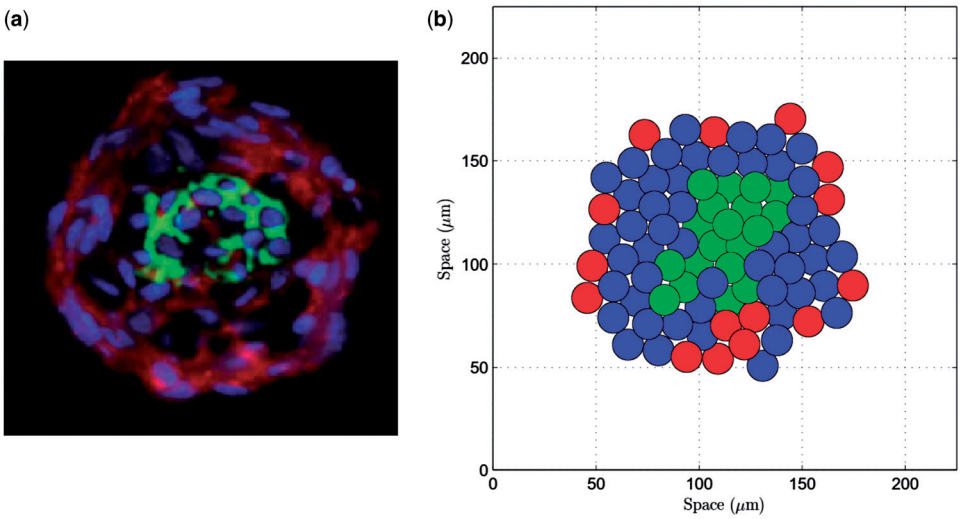

FIG. 1. (a) A CSp by immunofluorescence after 3 days: a cluster of immature stem cells (green) is localized in the central core of Cardiospheres, surrounded by differentiated supporting cells (red). Blue spots indicate cell nuclei, and cells inside the black area (non-labelled) are to be intended in an intermediate level of differentiation, see also Section 2 (source from Li *et al.*, 2010, by courtesy of John Wiley & Sons). (b) An example of a numerical simulation of our mathematical model showing a CSp at 3 days. Green, blue and red colours mark, respectively three increasing degrees of maturation of a single cell (see Section 4 for further details). [Colour only in the online version.]

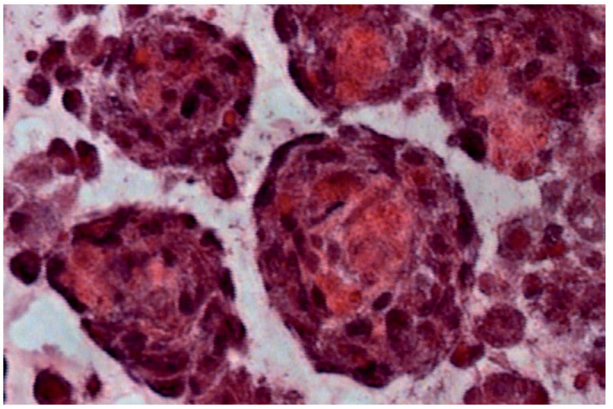

FIG. 2. Histological preparation of CSps ultra-thin slices. Haemathoxilin-eosin staining shows a nuclei-free central necrotic area more evident in larger CSps.

cell cycle inhibitors, neoangiogenesis, etc., and cannot be directly compared with those more limited of the adult cardiac progenitors. Nevertheless both of the 3D cellular growth mechanisms share some common features. CSps and neoplastic spheroids hold more than two functional phenotypes (proliferating, quiescent, differentiating, dying). The growth in a form of a 3D sphere limits the diffusion of the nutrients and oxygen and leads to the formation of a central core of death cells as a consequence of necrosis, apoptosis and anoichisis (Fig. 2). It is well known that in tumours the fastest proliferating cells are present in the intermediate and external layers forming the so-called growing front. On the contrary, in small and medium CSps the highest rate of the proliferation is observed in the central area due to the hypoxic conditions, which are closer to those corresponding to the pre-natal developing heart. However, while the spheres become larger the necrotic core appears as in tumours. In this article, we introduce a discrete in continuous non-deterministic model to simulate the growth of a CSp aggregate. We treat the various biological constituents using different levels of description: on the cellular scale we adopt a discrete description, while on the molecular scale chemical signals are considered as continuous variables (Anderson *et al.*, 2007; Preziosi & Tosin, 2009). This choice is justified by the relatively small number of cells involved in the formation of CSps, for which the hypothesis of the continuum does not hold, and by the much smaller size of the molecules with respect to them. Similar approaches have been adopted in analogous cell systems, for instance in relation to the modelling of tumour growth (Chaplain, 2011; Enderling *et al.*, 2012; Kim, 2013; Osborne *et al.*, 2015; Fletcher *et al.*, 2015, and references therein) or, recently, to describe the morphogenesis of the lateral line in the zebrafish embryo (Di Costanzo *et al.*, 2015a,b), and to study the behaviour of the collective motion of cells under chemotaxis and alignment effect (Di Costanzo & Natalini, 2015). With particular regards to the stem cell cultures, in Wu *et al.* (2014) a continuous diffusion–reaction mathematical model is proposed to investigate oxygen transport and distribution in embryonic stem cell aggregates, also in comparison with experimental data.

Our proposed mathematical model relies on a hybrid description: each cell is described separately by a system of ordinary differential equations, which take into account the self-organizing interactions between cells, through typical terms of collective dynamics and chemotaxis effects (see for instance the reviews by Vicsek & Zafeiris, 2012; Méhes & Vicsek, 2014); at a macroscopic level, by reaction–diffusion equations, we describe the concentrations of oxygen, as a representative of nutrients essential for cells metabolism, and of a growth factor TGF-β (transforming-growth-factor-β), as a chemoattractant and main regulator

of the cell differentiation, secreted by the cells and also present in the environment. Additionally, to model the formation of the Cardiosphere, we introduce two processes, the cell proliferation and differentiation, which lead to the growth and maturation of an initial cell cluster. We distinguish three differentiation levels of cell maturation, which also influence the two aforesaid processes. Moreover they are regulated by the local concentrations of oxygen and TGF-β. Another crucial feature of our model is the stochasticity. It is motivated by the so called noise in biological systems and the averaging of cells characteristics. The former is mainly due to the genetic diversity among individual cells, random collisions and thermal fluctuations in chemical reactions and randomness of various external factors, see Tsimring (2014). The latter concerns the simplifications introduced in our model, such as the uniform size of cells, equal maturation time or signal sensing. The randomness of the biological phenomena in our model is present in the proliferation and differentiation processes. When the necessary conditions are satisfied, cells divide or pass to a higher differentiated level with some probability, which increases if the conditions are favourable.

Using the proposed mathematical model, we have simulated the formation of a Cardiosphere in a 2D setting. After a careful sensitivity analysis of the model parameters, we were able to obtain numerical results comparable with the existing biological experiment: see again Fig. 1, in which the structure and composition of the two images, real experiment (a) and numerical simulation (b), are in good agreement. In order to meet the need of biological research and possible therapeutic applications (including the achievement of a more advanced differentiation level), we have analyzed the development of the Cardiosphere at two typical experimental concentration of oxygen.

The article is organized as follows: in Section 2, we present the general setting of the problem and the mathematical framework used throughout the article. In Section 3, we describe in detail the mathematical model for the cells and nutrients dynamics, together with the stochastic mechanisms of cell proliferation and differentiation. Section 4 contains the numerical results and relative biological interpretations. Finally, Section 5 is devoted to the conclusions and possible future perspectives.

2. Formulation of the problem

The in vitro 3D CSp formation starts from a low-density seeding of the explants-biopsy-derived cells in a defined culture conditions. First, adhered to the culture dish bottom the individual stem cells start to aggregate in small clusters of very few elements. Reaching certain dimensions they detach and grow immersed in a liquid environment and in a controlled gas atmosphere, which contain substances essential for their metabolism. In our model, we have reduced to two the biological and physical variables affecting the CSps growth and differentiation: the oxygen, representing nutrients and gases, and the TGF-β which is present in the culture medium and is produced by the cells themselves. The latter represents a key modulator of the main pathway involved in the induction of the non-terminal differentiation level achieved in our basic experimental conditions (Forte *et al.*, 2012). We assume that during the formation of a CSp, the cells are subject to two basic cellular processes, the proliferation and the differentiation, which depend, with some probability, on the type of a cell and on the local availability of oxygen. Moreover, we consider three different increasing differentiation levels for living cells and, separately, dead cells. The complex differentiation mechanism is triggered by a large enough concentration of TGF-β, is hindered by the presence in the closest proximity of a large number of cells of the same type and is inhibited when the concentration of oxygen drops below a threshold value (see Section 3.2).

To describe the formation of CSps in the next section, we propose a hybrid model, in which cells are considered as discrete entities while oxygen and TGF-β concentrations are continuum variables. We assume that in the absence of specific signals, the cell dynamics is due to attractive–repulsive forces and friction effect, taking place isotropically. The TGF-β, produced by the cells and also present in

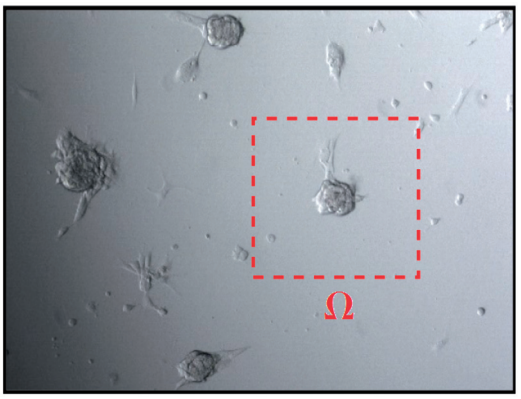

FIG. 3. Experimental picture of a culture of CSps. The dotted red line indicates the portion chosen as possible domain Ω for a single CSp in our mathematical model.

the external medium, is a chemoattractant for cell which moves towards its higher concentrations. For computational simplicityM, a two-dimensional description is adopted.

2.1 *Mathematical notations and operators*

In a Cartesian coordinate system, let us consider a rectangular domain Ω, which in our model represents a limited portion of the culture (containing many CSps) with a single cluster of stem cells in its centre (Fig. 3). For this reason in the following, we can assume periodic boundary condition in relation to the equations of the model. At the initial time, N_0 cells at the same maturation level (Section 3.2) and radius R (for simplicity all cells are assumed to have the same constant radius) are placed randomly at positions $\mathbf{X}_i$, $i = 1, 2, ..., N_0$ at the centr of the domain. In the following, due to proliferation, the number of cells at the time t will be denoted by $N(t)$. In the model, we denote by $c(\mathbf{x}, t)$ and $S(\mathbf{x}, t)$ the concentrations of oxygen and TGF-β, respectively, and in the numerical simulations these variables are discretized on a uniform spatial mesh. In general, the cell position $\mathbf{X}_i$ does not coincide with a mesh grid point, and we have to 'approximate' the value of $c(\mathbf{X}_i, t)$. In general, a cell 'feels' the presence of chemical substance (or a signal) $h(\mathbf{X}_i, t)$ not only at the centre $\mathbf{X}_i$, but also in its proximity. To model this graded influence, a weighted average operator is defined:

$$\mathcal{F}(h(\mathbf{X}_i, t)) = \frac{1}{W} \int_{B(\mathbf{X}_i, \bar{R})} w_i(\mathbf{x}) h(\mathbf{x}, t)\, d\mathbf{x}, \tag{2.1}$$

where:

$$W := \int_{B(\mathbf{X}_i, \bar{R})} w_i(\mathbf{x})\, d\mathbf{x}, \tag{2.2}$$

and a possible choice for the weight function can be a truncated Gaussian

$$w_i(\mathbf{x}) := \begin{cases} 2 \exp\left(-||\mathbf{x} - \mathbf{X}_i||^2 \dfrac{\log 2}{\bar{R}^2}\right) - 1, & \text{if } ||\mathbf{x} - \mathbf{X}_i|| \le \bar{R}, \\ 0, & \text{otherwise,} \end{cases}$$

which models a sensing intensity decreasing on the distance from the cell centr. Here $\bar{R}$ represents an influence radius, possibly greater than the cell radius R (Table 2), and

$$B(\mathbf{X}_i, R) := \{\mathbf{x} : ||\mathbf{x} - \mathbf{X}_i|| \leq R\}$$

is the ball centred in $\mathbf{X}_i$ with radius R. In the following, the characteristic function over the ball $B(\mathbf{X}_i, R)$ is defined as:

$$\chi_{B(\mathbf{X}_i,R)} := \begin{cases} 1, & \text{if } \mathbf{x} \in B(\mathbf{X}_i, R), \\ 0, & \text{otherwise.} \end{cases}$$

3. The mathematical model

In this section, we present in detail the discrete in continuous model for the formation of a Cardiosphere. Firstly, we present the equations describing the movement of cells and the forces acting on them. Then we focus on the proliferation and differentiation processes. The basic mechanisms of the phenomena are explained and the reaction–diffusion systems for the time evolution of the oxygen and TGF-β concentrations are given.

3.1 *Cells dynamics*

Motion of cells is the result of mechanical forces acting on them and of their reciprocal interactions. Due to the finite volume of cells, there is an internal pressure between them which leads to repulsion while being compressed. On the other hand, there are attractive bonds between cells which keep them in contact. We also assume that cells are driven by a chemotactic signal, that is they move towards the higher gradient of the TGF-β concentration and are slowed down because of the viscosity of the medium in which they are immersed (Rubinstein *et al.*, 2009; Fournier *et al.*, 2010; Bayly *et al.*, 2012).

The position of the ith cell $\mathbf{X}_i$ follows Newton's law and is described by the second order ordinary differential equation

$$\ddot{\mathbf{X}}_i = \sum_{j:\mathbf{X}_j \in B(\mathbf{X}_i,R_2)\setminus\{\mathbf{X}_i\}} \mathbf{K}(\mathbf{r}_{ij}) - \mu\dot{\mathbf{X}}_i + \alpha\mathcal{F}(\nabla S(\mathbf{X}_i, t)), \tag{3.1}$$

where dot denotes time derivative, μ is a friction coefficient for unit mass and $\mathbf{K}(\mathbf{r}_{ij})$ is the attraction-repulsion force for unit mass between ith and jth cell, defined as

$$\mathbf{K}(\mathbf{r}_{ij}) := \begin{cases} -k_1\left(\dfrac{1}{||\mathbf{r}_{ij}||} - \dfrac{1}{R_1}\right)\dfrac{\mathbf{r}_{ij}}{||\mathbf{r}_{ij}||}, & ||\mathbf{r}_{ij}|| \leq R_1, \\ \\ k_2(||\mathbf{r}_{ij}|| - R_1)\dfrac{\mathbf{r}_{ij}}{||\mathbf{r}_{ij}||}, & R_1 < ||\mathbf{r}_{ij}|| \leq R_2. \end{cases} \tag{3.2}$$

The parameters k_1, k_2 are positive constants, $\mathbf{r}_{ij} = \mathbf{X}_j - \mathbf{X}_i$ is the distance between cells, $R_1 = 2R$ and R_2 (to be chosen later, see Table 2) are the radii of repulsion and attraction, respectively. Note that equation $(3.2)_1$ gives a repulsion in the form $1/r$, while $(3.2)_2$ is a linear attractive elastic force. Similar terms

can be found in the model proposed in D'Orsogna *et al.* (2006); Joie *et al.* (2015). Equation (3.1) is augmented with the initial conditions

$$\mathbf{X}_i(0) = \mathbf{X}_i^0, \qquad \mathbf{X_i}(0) = \mathbf{V}_i^0 = \mathbf{0}.$$

3.2 *Proliferation and differentiation*

Some of the present authors have been investigating the proliferation and differentiation dynamics of cells forming CSps from the original description of the method of isolation and expansion of human cardiac progenitors from heart biopsy (Messina *et al.*, 2004). Confocal analysis of the cells labelled with Bromodeoxyuridine, which incorporate the base analogue within the replicating DNA, showed the positive fluorescence labelled cells located in the inner of the growing spheres. No or a weak signal was present in the external layers of more differentiated cells (that cannot replicate at the same speed). This kind of layered growth implies that the proliferation in the central area depends also on the CSps size and the core-cells may become quiescent or die by necrosis or apoptosis.

It is worth noting that tumour spheroid growth depends (at least partially) on the same factors, however, in this case they show a more pronounced variety of final volumes for any given cell line. We can distinguish an early phase of global undifferentiated mass, a second stage of a shell of proliferating cells around a central area of quiescent elements and the last stage in which an inner necrotic/apoptotic core is enveloped by the previous two. The external layer always represents the growing front (Kim, 2013).

Stem cells are characterized by different levels of maturation (differentiation). To model this feature, we mark the i-cell with a label $\varphi_i(t) = 1, 2, 3, d$, called its 'state'. The state $\varphi = d$ indicates dead cells or the space occupied by necrotic mass (due to adverse biological conditions, as oxygen deficiency for a sufficiently long period of time). Note that apoptosis, which is a programmed cells death, occurs over a longer timescale and is not considered here. In particular, we introduce a threshold concentration c_d such that whenever $\mathcal{F}(c(\mathbf{X}_i, t)) > c_d$ cell survives, otherwise it dies. Such cell is marked as dead ($\varphi = d$) and does not take part in further evolution of the CSp, that is it neither proliferates nor differentiates. However, dead cells do occupy a volume and exert attractive-repulsive forces on other cells. A stochastic process introduced in the process of proliferation and differentiation models also the presence of quiescent cells. Such cells neither proliferate nor differentiate but, in contrast to dead cells, this state results from environment conditions and is only temporary. At a later time, a quiescent cell can restart its functions.

For a living cell, $\varphi = 1$ denotes the lowest degree of maturation (the least differentiated cells), while $\varphi = 2, 3$ are the intermediate and the highest degrees of differentiation, respectively. They can be experimentally reached with our previously cited method (Messina *et al.*, 2004; Chimenti *et al.*, 2012). Finally, we define a *cell cycle time* T_c, i.e. a cell maturation time after which the cell may proliferate and/or differentiate with some probability.

3.2.1 *Mechanism of differentiation*

In the model we assume that, with some probability and when *environment* conditions are satisfied, from time t to time $t + \Delta t$ a cell can change its state to a higher one by a unity according to Table 1, or can die (as described in Section 3.2.2).

More precisely, the differentiation is triggered by chemical signals, such as TGF-β present in the extracellular environment and secreted by cells themselves. Moreover, it can be inhibited due to the presence, in the surrounding area, of cells of the same type, as we can found in similar cell systems

TABLE 1 *Possible differentiation levels reached by a cell. The check marks the admissible transition at time $t + \Delta t$ for each cell state on the first column*

	$\varphi_i(t+\Delta t)=1$	$\varphi_i(t+\Delta t)=2$	$\varphi(t+\Delta t)=3$
$\varphi_i(t)=1$	✓	✓	
$\varphi_i(t)=2$		✓	✓
$\varphi_i(t)=3$			✓

(Itoh & Chitnis, 2001; Matsuda & Chitnis, 2010) and mathematical models (e.g. Di Costanzo *et al.*, 2015a). We denote by Γ_i an inhibitor indicator function, which depends on the number n_i of cells in the neighbourhood of the ith cell and is defined as

$$\Gamma_i(t) = \begin{cases} 1, & \text{if } n_i \le \bar{n}, \\ 0, & \text{if } n_i > \bar{n}, \end{cases} \qquad n_i := \text{card}\{j : \mathbf{X}_j \in B(\mathbf{X}_i, R_4)\}, \qquad i = 1, \dots, N.$$

For the threshold $\bar{n}$, we set in the following the value $\bar{n} = 4$ for a 2D case.

We define a differentiation threshold

$$q_i(t) := \frac{\sigma(\varphi_i) \cdot \mathcal{F}(S(\mathbf{X}_i, t)) \cdot \Gamma_i(t)}{S_{\max}}, \qquad i = 1, \dots, N, \tag{3.3}$$

for the cell i, with $\sigma(\varphi_i)$ ($\varphi_i = 1, 2$) positive constants, and $S_{\max}$ the experimental maximum value of TGF-β (Table 2). In addition, we assume that differentiation occurs under the condition that oxygen concentration level is above a given threshold value $\bar{c}(\varphi_i)$, also depending on the cell states $\varphi_i = 1, 2$.

The differentiation variable $\varphi_i(t)$ can be modelled as a non-homogeneous Poisson process with variable intensity $q_i(t)$ (see e.g. Anderson *et al.*, 2015 and references therein, as well as Kusher & Dupuis, 1992). In particular, the probability of a differentiation in a time interval Δt is given by

$$P(\varphi_i(t + \Delta t) - \varphi_i(t) \ge 1) \cong q_i(t)\Delta t, \tag{3.4}$$

the expected number of differentiations in the interval $(t, t + \Delta t)$ is

$$E\,(\text{number of differentiations in } (t, t + \Delta t)) = q_i(t)\Delta t, \tag{3.5}$$

therefore in the time interval $(0, t)$ results

$$E\,(\text{number of differentiations in } (0, t)) = \int_0^t q_i(s)\, ds. \tag{3.6}$$

Finally, we write the stochastic equation

$$d\varphi_i = d\mathcal{P}\left(\int_0^t q_i(s)\, ds\right), \quad i = 1, \dots, N, \tag{3.7}$$

$\mathcal{P}(\int_0^t q_i(s)\, ds)$ being a inhomogeneous Poisson process with intensity $q_i(t)$.

In practice, if $\mathcal{F}(c(\mathbf{X}_i,t)) \geq \bar{c}(\varphi_i)$, starting from (3.7), we compute the threshold (3.3), and we can adopt the following stochastic rule: cell types $\varphi_i = 1$ and $\varphi_i = 2$ switch irreversibly their state according to

$$\varphi_i(t+\Delta t) = \varphi_i(t) + \begin{cases} 1, & \text{if } \bar{q}_i < q_i \Delta t, \\ 0, & \text{otherwise,} \end{cases} \qquad i = 1,\dots,N, \tag{3.8}$$

where $\bar{q}_i$ is a random number between 0 and 1 (see also Section 4).

Although different scenarios can be envisaged, here we assume that after differentiation, the cell time is reset and a subsequent differentiation may occur after the cell cycle T_c, according to the aforesaid Poisson process. The same holds for the proliferation mechanism described in the next Section 3.2.2.

3.2.2 *Mechanism of proliferation* We introduce the proliferation thresholds $p_i(t)$ of the ith cell at time t in the following form

$$p_i(t) = \begin{cases} g_1(\mathcal{F}(c)), & \text{if } \varphi_i(t) = 1, \\ g_2(\mathcal{F}(c)), & \text{if } \varphi_i(t) = 2, \\ g_3(\mathcal{F}(c)), & \text{if } \varphi_i(t) = 3. \end{cases} \tag{3.9}$$

Functions g_1, g_2, g_3 describe the dependence of the rate of proliferation on the concentration of oxygen. Least differentiated cells, i.e. those at state $\varphi = 1$, work under anaerobic conditions. Their proliferative ability increases at low levels of oxygen with an assumed Gaussian-type dependence. When c is too high, cells change their metabolism and proliferate at a lower rate. Cells at states $\varphi = 2, 3$ behave on the opposite: their proliferation rate increases with higher concentration of oxygen. However, due to the fact that they are already differentiated, their ability to proliferate is lower than the stem cells at $\varphi = 1$. As a consequence, a possible choice for functions g_1, g_2, g_3, used in the numerical simulations, is shown in Fig. 4. Explicit formulas for $g_{1,2,3}$ functions are given in Appendix. If, for certain interval of time, the concentration of oxygen is below a given threshold c_d, then cells do not have enough resources to live and die.

To model stochasticity in proliferation, we introduce a new state variable $\phi_i(t)$ denoting the number of (from $i-th$) generated cells in $(0,t)$. Similarly to the differentiation (Section 3.2.1), $\phi_i(t)$ satisfies a non-homogeneous Poisson process:

$$d\phi_i = d\mathcal{P}\left(\int_0^t p_i(s)\,ds\right), \quad i = 1,\dots,N, \tag{3.10}$$

with variable intensity $p_i(t)$ given by equation (3.9).

If $\mathcal{F}(c(\mathbf{X}_i)) > c_d$, we compute the proliferation threshold of the ith cell p_i through equation (3.9). The following computational rule of proliferation is applied:

$$\phi_i(t+\Delta t) = \phi_i(t) + \begin{cases} 1, & \text{if } \bar{p}_i < p_i \Delta t, \\ 0, & \text{otherwise,} \end{cases} \qquad i = 1,\dots,N, \tag{3.11}$$

where $\bar{p}_i$ is a random number between 0 and 1 (see also Section 4).

When a cell proliferates, a newborn $(N+1)$th cell appears and is appended to the vector of coordinates $\mathbf{X}_i$, $i = 1,2,\dots,N$. Its position $\mathbf{X}_{N+1}$ is generated randomly within the distance r from the mother cell

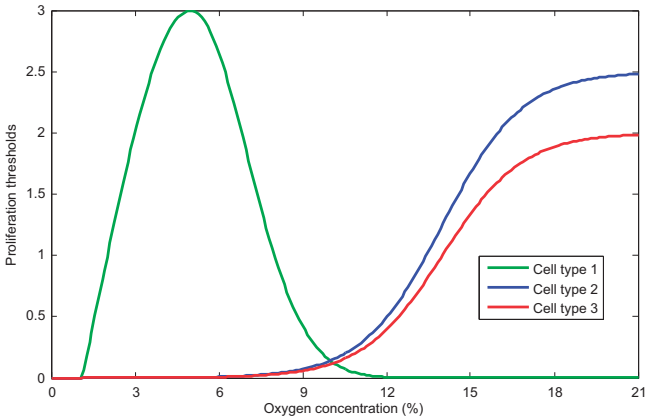

FIG. 4. Proliferation thresholds as a function of oxygen concentration (equation (3.9)).

and with same velocity. More precisely, in polar coordinates we choose randomly two numbers: the angle $\theta \in [0, 2\pi]$ and the distance between the two centrs $r \in [R/2, R]$.

3.3 *Dynamics of oxygen and TGF-β signal*

The concentration of oxygen $c = c(\mathbf{x}, t)$ is a continuous variable and its time evolution is governed by a reaction–diffusion equation:

$$\begin{cases} \partial_t c = \nabla \cdot (D_c \nabla c) - \displaystyle\sum_{i=1}^{N} \frac{\lambda(\varphi_i) c^{\gamma+1}}{k(\varphi_i) + c^{\gamma+1}} \chi_{B(\mathbf{x}_i, R_3)} + H\bar{B}(c_0 - c), & \\ c(\mathbf{x}, 0) = c_0, & \text{in } \Omega, \\ \text{periodic boundary conditions}, & \text{on } \partial\Omega, \end{cases} \tag{3.12}$$

with c_0 the environmental (constant) concentration. The last term in equation $(3.12)_1$ models the 2D representation of the real 3D experiment: the supply of oxygen coming from the environment (upper surface of the culture) is recovered as a source term, modelled as proportional to the difference $c_0 - c$ with rate H, and spatially modulated by a well-shaped function over the CSp geometry, in the form

$$\bar{B}(\mathbf{x}) := \begin{cases} \dfrac{\exp\left[\zeta \left(\dfrac{r(\mathbf{x})}{R_{\mathrm{CSp}}}\right)^2\right] - 1}{\exp(\zeta) - 1}, & \text{if } r \le R_{\mathrm{CSp}}, \\ 1, & \text{otherwise.} \end{cases} \tag{3.13}$$

The constant ζ is a geometrical parameter, $r(\mathbf{x})$ is the distance from the centr of the sphere, and R_{CSp} is the mean radius of CSp at time t. The shaped function (3.13) considers the graded exposition to oxygen of cells at different depth. In the equation (3.12), we assume that oxygen diffuses in the environment and is consumed by cells with a rate depending on the metabolism of the cell (i.e. on its state φ_i), and

increases with the oxygen availability ($\propto c^{\gamma}$, $\gamma > 0$) according to the saturation Michaelis–Menten-like law (Wu *et al.*, 2014). A typical value $\gamma = 1/2$ is assumed. Degradation of the oxygen is negligible over the typical time scale (few days) of the experiment.

The concentration of the chemical signal $S(\mathbf{x}, t)$ is governed by the similar IBV problem

$$\begin{cases} \partial_t S = \nabla \cdot (D_S \nabla S) + \displaystyle\sum_{i=1}^{N} \xi(\varphi_i)\chi_{B(\mathbf{X}_i,R_3)} - \eta S, & \\ S(\mathbf{x}, 0) = S_0, & \text{in } \Omega, \\ \text{periodic boundary conditions}, & \text{on } \partial\Omega, \end{cases} \tag{3.14}$$

where ξ is the (state dependent) S-release rate, η is the molecular degradation rate and $D_S(\mathbf{x})$ is a diffusion coefficient. Compared with the production term, a possible S-consumption term is extremely low and has been neglected.

In addition, the diffusivity coefficient D (say D_c in equation (3.12), D_S in (3.14)) varies in relation with the change of cell density, which we measured in a reference volume. Due to the presence of a large number of cells, D is significantly reduced at the centre of the CSp. Diffusion can be considered as in a porous medium, and the *effective diffusivity* $D(\mathbf{x})$ can be defined as:

$$D(\mathbf{x}) := \frac{D^{\max}}{1 + \rho \bar{A}(\mathbf{x})}, \tag{3.15}$$

where $D^{\max}$ is the constant unperturbed diffusion, ρ is a compactness parameter and $\bar{A}(\mathbf{x})$ is the occupancy fraction in a proper control volume containing $\mathbf{x}$.

4. Numerical results and discussion

In this section, we present numerical simulations of a typical formation and growth of CSps, under typical conditions (Messina *et al.*, 2004; Chimenti *et al.*, 2012), using the previously described mathematical model.

For convenience, we summarize here our hybrid system of equations:

$$\begin{cases} \ddot{\mathbf{X}}_i &= \displaystyle\sum_{j:\mathbf{X}_j \in B(\mathbf{X}_i,R_2)\setminus\{\mathbf{X}_i\}} \mathbf{K}(\mathbf{r}_{ij}) - \mu\dot{\mathbf{X}}_i + \alpha\mathcal{F}(\nabla S(\mathbf{X}_i)), \\ d\varphi_i &= d\mathcal{P}\left(\displaystyle\int_0^t q_i(s)\,ds\right), \\ d\phi_i &= d\mathcal{P}\left(\displaystyle\int_0^t p_i(s)\,ds\right), \\ \partial_t c &= \nabla \cdot (D_c \nabla c) - \displaystyle\sum_{i=1}^{N} \frac{\lambda(\varphi_i)c^{\gamma+1}}{k(\varphi_i) + c^{\gamma+1}}\chi_{B(\mathbf{X}_i,R_3)} + H\bar{B}(c_0 - c), \\ \partial_t S &= \nabla \cdot (D_S \nabla S) + \displaystyle\sum_{i=1}^{N} \xi(\varphi_i)\chi_{B(\mathbf{X}_i,R_3)} - \eta S, \end{cases} \tag{4.1}$$

where $\mathbf{K}(\mathbf{r}_{ij})$ and $\mathcal{F}(\nabla S(\mathbf{X}_i))$ are given, respectively in (3.2) and (2.1), while q_i and p_i given by (3.3) and (3.9). Initial and boundary conditions are given by:

$$\begin{aligned}
\mathbf{X}_i(0) &= \mathbf{X}_i^0, \qquad \dot{\mathbf{X}}_i(0) = \mathbf{0}, \\
N(0) &= N_0, \qquad \varphi_i(0) = 1, \qquad \forall i = 1, \ldots, N_0, \\
c(\mathbf{x}, 0) &= c_0, \qquad \text{periodic boundary conditions on } \partial\Omega, \\
S(\mathbf{x}, 0) &= S_0, \qquad \text{periodic boundary conditions on } \partial\Omega.
\end{aligned}$$

Initially, we consider a cluster of $N_0 = 15$ cells at the first stage of differentiation ($\varphi_i = 1, \forall i$) placed at the centre of a square domain $\Omega = [0, 225] \times [0, 225]$ (μm^2). Such setting models the initiation of the numerical simulation at the time that corresponds to about 24 h of the real experiment.

Despite the low geometrical dimension and a number of simplifying assumptions, the large set of biological parameters influences the problem and their complete characterization remains a difficult task. Each parameter is interconnected with the others and strongly affects the simulation. Some of them are taken from previously published results or literature, others are chosen in a compatible and consistent range, and the remaining ones are varied to analyze the sensitivity of the system. The complete set of biological parameters is given in Table 2.

4.1 *Numerical methods*

All the equations are discretized by finite differences. The second order equation $(4.1)_1$ is reduced to a system of first order equations and solved by explicit Euler in time. In equations $(4.1)_{4,5}$ the diffusion terms are discretized by a standard centred difference in space and integrated implicitly in time. The non-linear reaction terms are treated explicitly in time. Finally, in equation $(4.1)_5$ we have eliminated the stiff term $-\eta S$ using a classical exponential transformation.

The square domain size is chosen sufficiently large, 225 μm per side, so that the growing CSp does not reach the boundary in the typical time of observation. We consider an uniform mesh with grid spacing $\Delta x = \Delta y = 3.75\,\mu$m ($60 \times 60$ grid points), which guarantees a sufficient discretization over each cell (having a diameter of 15 μm, see Table 2) and a reasonable accuracy.

The time step Δt has been fixed as the maximum value to ensure stability and non-negativity of the scheme (max $\Delta t = 0.02$ h). For the same reason, when the oxygen concentration drops below a given threshold, it is necessary to reduce the time step to $\Delta t = 0.001$ h.

A convergence analysis performed on finer meshes, respectively $\Delta x = \Delta y = 2.8125\,\mu$m ($80 \times 80$ grid points) and $\Delta x = \Delta y = 2.25\,\mu$m ($100 \times 100$ grid points), demonstrated the mesh independence of the numerical results (data not shown).

The construction of the initial data for cells, the approximation of the equations of motion for cells, of the reaction–diffusion equations for TGF-β and oxygen and the numerical code for the proliferation/differentiation processes are detailed in the Appendix.

4.2 *Parameter sensitivity analysis*

Mathematical models of biological phenomena are subject to sources of uncertainty, including errors of measurement, natural intrinsic variability of the system, absence of information and poor or partial understanding of the driving forces and mechanisms. This uncertainty imposes a limit on our confidence in the response or output of the model. One of the challenges is to characterize the model

TABLE 2 *Estimates of physical and biological parameter values. Whenever possible, the values are taken from literature or experiments, the remaining are calibrated to be consistent with other (c.w.o.). Their influence on the system is studied through a local sensitivity analysis (Section 4.2). When a parameter admits a range of possible values, the used one in the numerical tests is put in brackets*

Parameter	Definition	Estimated value or range (used values)	Source
R	Cell radius	7.5 μm	Wu *et al.* (2014)
$\bar{R}$	Detection radius of chemicals	2R	Biological assumption
R_1	Radius of action of repulsion between cells	2R	Biological assumption
R_2	Radius of action of adhesion between cells	2.5R	Biological assumption
R_3	Radius of production/degradation of chemicals	R	Biological assumption
R_4	Detection radius for the differentiation inhibition	2R	Biological assumption
α	Coefficient of chemotactic effect per unit mass	10^{10} μm^4 h^{-2}pg^{-1}	Calibrated, c.w.o.
k_1	Coefficient of repulsion per unit mass	10^{17} μm^2 h^{-2}	Calibrated, c.w.o.
k_2	Elastic constant per unit mass	$1.29 \times 10^{14} - 1.29 \times 10^{19}$ (1.29×10^{14}) h^{-2}	Bell *et al.* (1984)
μ	Friction coefficient per unit mass	$5.82 \times 10^{14} - (5.82 \times 10^{15})$ h^{-1}	Rubinstein *et al.* (2009)
$D_c^{\max}$	Oxygen diffusion coefficient	$3.72 - 4.93$ $(4.32) \times 10^6 \mu$m^2 h^{-1}	Wu *et al.* (2014)
$D_S^{\max}$	TGF-β diffusion coefficient	$9.36 \times 10^4 \mu$m^2 s^{-1}	AIS Project (2001)
$\xi(\varphi_{1,2,3})$	Coefficient of production of TGF-β	$2.7 \times 10^{-8} - 1.1 \times 10^{-6}$ (5.64×10^{-7}) pg μm^{-2} h^{-1}	Chimenti *et al.* (2010)
$S_{\max}$	Maximum concentration of TGF-β	3×10^{-8} pg μm^{-2}	Chimenti *et al.* (2010)
η	Degradation constant of TGF-β	$13.86 - 20.79$ (17.33) h^{-1}	Wakefield *et al.* (1990)
$\sigma(\varphi = 1, 2)$	Differentiation constant	50 (if $\varphi = 1$), 2.5 (if $\varphi = 2$) (nondim.)	Calibrated, c.w.o.
$g_{1,2,3}^{\max}$	Maximum of functions g_1, g_2, g_3 in Fig. 4	3 (if $\varphi = 1$), 2.5 (if $\varphi = 2$), 2 (if $\varphi = 3$) (nondim.)	Calibrated, c.w.o.
$\lambda(\varphi = 1, 2, 3)$	Oxygen consumption constant	$0.9 \times 10^{-2} - 2.52 \times 10^{-2}$ (1.4×10^{-2} if $\varphi = 1$, 2.5×10^{-2} if $\varphi = 2$, 2.5×10^{-2} if $\varphi = 3$) pg μm^{-2} h^{-1}	Wu *et al.* (2014)
$k(\varphi = 1, 2, 3)$	Michaelis–Menten oxygen constant	1.67×10^{-5} pg μm^{-2}	Wu *et al.* (2014)
$\bar{c}(\varphi = 1, 2)$	Oxygen concentration threshold value for diff.	4×10^{-4} (if $\varphi = 1$), 28×10^{-4} (if $\varphi = 2$) pg μm^{-2}	Calibrated, c.w.o.
c_d	Oxygen minimum concentration for life (necrosis)	1.93×10^{-4} pg μm^{-2}	Wu *et al.* (2014)
c_0	Environmental concentration for oxygen	3.68×10^{-3} pg μm^{-2} (if O_2 at 21%), 8.83×10^{-4} pg μm^{-2} (if O_2 at 5%)	Wu *et al.* (2014)
S_0	Environmental concentration for S	6.62×10^{-9} pg μm^{-2}	Thermo Scientific (2007)
T_c	Cell cycle time	15 h (if O_2 at 21%), 12 h (if O_2 at 5%)	Messina *et al.* (2004)
H	Source rate	40 h^{-1}	Calibrated, c.w.o.
ρ	Compactness parameter	9×10^3 (nondim.)	Calibrated, c.w.o.

parameters that are not identified experimentally, and these parameters are marked as *calibrated* in Table 2.

In this section, we present the calibration procedure in order to obtain as reliable results as possible. To achieve this goal, we studied the influence of the parameters on the model dynamics through a local sensitivity analysis (Saltelli *et al.*, 2008; Clarelli *et al.*, 2015). This approach determines a degree of dependency between input parameters (one at a time) and the results of simulations. Although our analysis does not take into account the presence of interactions between parameters, as in the global sensitivity analysis, it can give useful information for further exploration of the parameter space.

We measure the sensitivity of the model to the variation of a positive quantity Ψ with respect to a reference parameter p_0 by defining a sensitivity index $SV \geq 0$ as:

$$SV := \frac{|\bar{\Psi}(p_0 \pm \varepsilon) - \bar{\Psi}(p_0)|/\bar{\Psi}(p_0)}{\varepsilon/p_0}, \tag{4.2}$$

where $\bar{\Psi}$ is the average value of Ψ over a large number of runs (100 in our analysis) and it accounts for the stochasticity presents in our model. Typically, ε is a small deviation over p_0 ($\varepsilon = 0.05p_0$, i.e. 5% variation). In Table 3, we report the sensitivity index computed with respect to two observed variables: the total number of cells N, and the diameter of the CSp, both at the final simulated time of 72 h. The smallness of the index gives us confidence of the robustness of the model in the response of the system in the presence of uncertainty.

4.3 *Simulations: growth and maturation of the CSp*

We performed numerical simulations of growth and differentiation of CSp considering the O_2 and TGF-β as the only key-regulatory biological mechanism. We compared the composition and the structure of the CSp at two typical experimental oxygen conditions.

First, we analyzed the normal culture condition which corresponds to the 21% concentration of the oxygen O_2. The state of the CSp at the initial and three following times is presented at Fig. 5. Differentiation levels are marked by different colours: green for the least differentiated cells ($\varphi = 1$), blue colour is for the intermediate level of differentiation ($\varphi = 2$), while the red colour labels cells with the highest degree of maturation ($\varphi = 3$). The reported results are in good agreement with the biological observations. We reproduced the CSp biological system consisting of a central core of less differentiated but faster proliferating cells surrounded by more specialized ones. The oxygen and TGF-β concentrations at different times are shown in Fig. 6.

Then we considered the hypoxic culture conditions in the CSp environment, that is the 5% oxygen concentration. The corresponding structure and composition of CSp, shown in Fig. 7, match the real situation. The size of the sphere is larger than that experimentally observed, because of the equally circular shape of cells and their constant radius in our model.

To compare and summarize the above results, we show in Fig. 8(a) in the form of pie charts the cell composition after 72 h in the two above cases. Similarly, Fig. 8(b) presents the growth of CSp diameter, and Fig. 8(c)–8(d) the time evolution of the ratio between the total mass at time t and the initial mass, $m_{\text{rel}}(t) := m(t)/m(0)$, respectively for oxygen and TGF-β. We observe that the oxygen levels decrease more at the hypoxic conditions (5%) due to the increased proliferation and, as a result, initially the diameter of the sphere at 5% is larger than at 21%. However, the increasing deficiency of the oxygen lead to the formation of the necrotic core and the slower growth. Because of the initial condition equal for each

TABLE 3 *Local sensitivity index SV as defined in equation (4.2) with ε corresponding to a 5% variation, computed for the parameters used in the numerical simulations and marked as calibrated in Table 2. The average values have been taken on 100 independent runs, in the case of oxygen at 21%. Observed variables N and the CSp diameter have been considered at the final time of 72 h. In the first row for N and for the diameter, the reference average value and the standard deviation are shown*

	N		Diameter	
	Average = 73.31		Average = 123.28 μm	
Parameters changed	(Standard deviation = 13.42 %)	SV_N	(Standard deviation = 5.71%)	SV_{diameter}
$\alpha + \varepsilon$	−0.68 %	0.14	−0.21%	0.04
$\alpha - \varepsilon$	−1.28 %	0.26	−0.83%	0.17
$\bar{c}(\varphi_1) + \varepsilon$	−2.08 %	0.41	−1.38%	0.27
$\bar{c}(\varphi_1) - \varepsilon$	−1.28 %	0.26	−0.83%	0.16
$\bar{c}(\varphi_2) + \varepsilon$	+0.31 %	0.06	+0.36%	0.07
$\bar{c}(\varphi_2) - \varepsilon$	+0.29 %	0.06	-0.51%	0.10
$H + \varepsilon$	−0.29 %	0.06	−0.30%	0.06
$H - \varepsilon$	+2.74 %	0.55	−0.73%	0.14
$k_1 + \varepsilon$	+0.79 %	0.16	+0.40%	0.08
$k_1 - \varepsilon$	−0.28 %	0.05	−2.57%	0.51
$k + \varepsilon$	+0.87 %	0.17	−0.05%	0.01
$k - \varepsilon$	−0.25 %	0.05	−1.19%	0.24
$\sigma(\varphi_1) + \varepsilon$	−1.36 %	0.27	−1.15%	0.23
$\sigma(\varphi_1) - \varepsilon$	−1.87 %	0.37	−1.43%	0.29
$\sigma(\varphi_2) + \varepsilon$	−2.63 %	0.53	−0.83%	0.17
$\sigma(\varphi_2) - \varepsilon$	+0.87 %	0.17	−0.83%	0.17
$\rho + \varepsilon$	+0.80 %	0.16	−0.70%	0.13
$\rho - \varepsilon$	−0.53 %	0.10	−0.76%	0.15
$\lambda(\varphi_1) + \varepsilon$	+1.32 %	0.26	−1.55%	0.31
$\lambda(\varphi_1) - \varepsilon$	−2.55 %	0.51	−0.84 %	0.16
$\lambda(\varphi_2) + \varepsilon$	+1.80 %	0.36	−0.15%	0.03
$\lambda(\varphi_2) - \varepsilon$	−2.01 %	0.40	−1.01 %	0.20
$g_1^{\max} + \varepsilon$	−0.74 %	0.15	−0.59%	0.12
$g_1^{\max} - \varepsilon$	+1.48 %	0.29	+0.05%	9.1×10^{-3}
$g_2^{\max} + \varepsilon$	−0.47 %	0.10	−0.78%	0.16
$g_2^{\max} - \varepsilon$	−3.36 %	0.67	−0.89%	0.18
$g_3^{\max} + \varepsilon$	−0.22%	0.04	−0.88%	0.18
$g_3^{\max} - \varepsilon$	+0.23 %	0.05	+0.04 %	9.1×10^{-3}

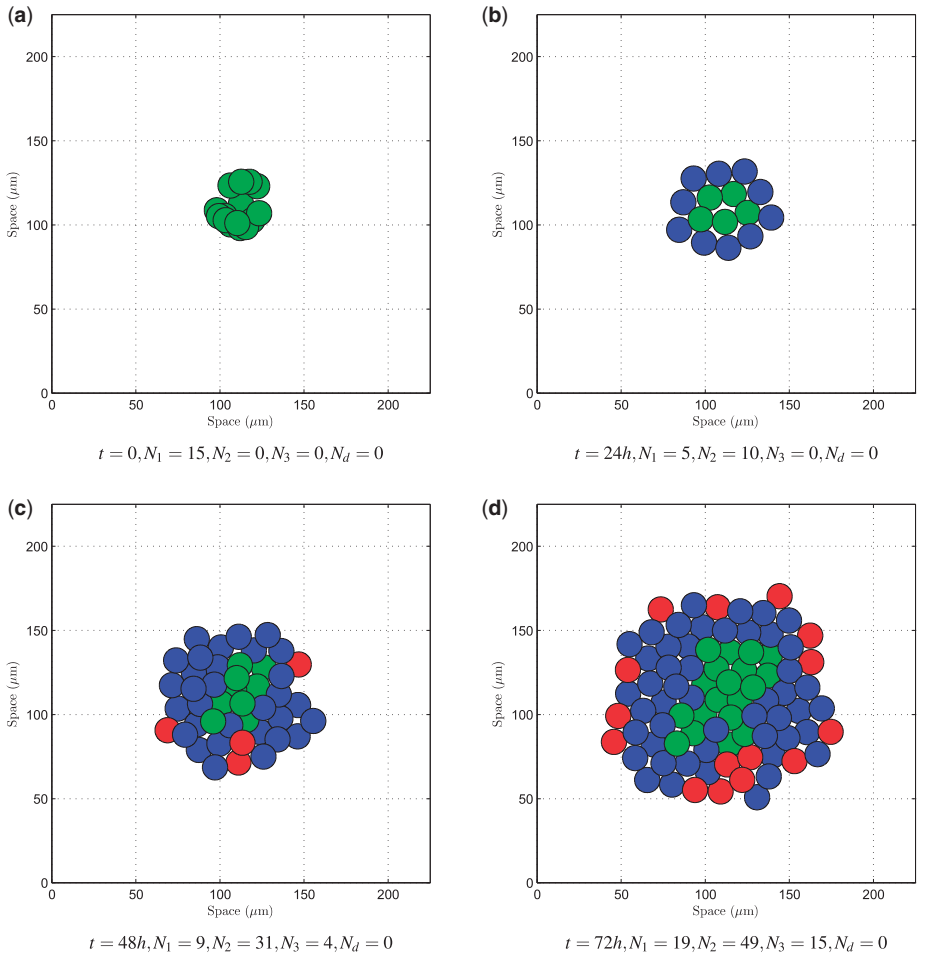

FIG. 5. (a)–(d) Numerical simulation of the CSp growth for a 21% oxygen environmental concentration, at times $t = 0, 24, 48, 72$ h. System (4.1) is solved in a domain $\Omega = [0, 225] \times [0, 225]$ (μm^2), with the model parameters given by Table 2. Differentiation levels are marked by different us: green for the least differentiated cells ($\varphi = 1$), blue colour is for the intermediate level of differentiation ($\varphi = 2$), while the red colour labels cells with the highest degree of maturation ($\varphi = 3$). Values N_1, N_2, N_3, N_d, in the subplot captions indicate the numbers of cells in the CSp, respectively for each state of maturation and for dead cells, $\varphi = 1, 2, 3, d$. [Colour only in the online version.]

cell and equal maturation time, cells undergo a higher degree of synchronization. As a result we observe the characteristic steps in the curves describing the growth of the CSp diameter, in correspondence of the beginning of the proliferation cycle.

The proposed model appears to be in a good agreement with the observed biological experiments at hand (Messina *et al.*, 2004; Chimenti *et al.*, 2012). We were able to reproduce the basic structures of CSps at two different oxygen concentration levels. In case of 21% of the environmental concentration, we observed the central region with proliferating, undifferentiated cells and the external ring of less multiplicating but differentiating cells. On the other hand, at 5% an evident necrotic core is observed, without many cells at higher differentiation level in the surrounding layers.

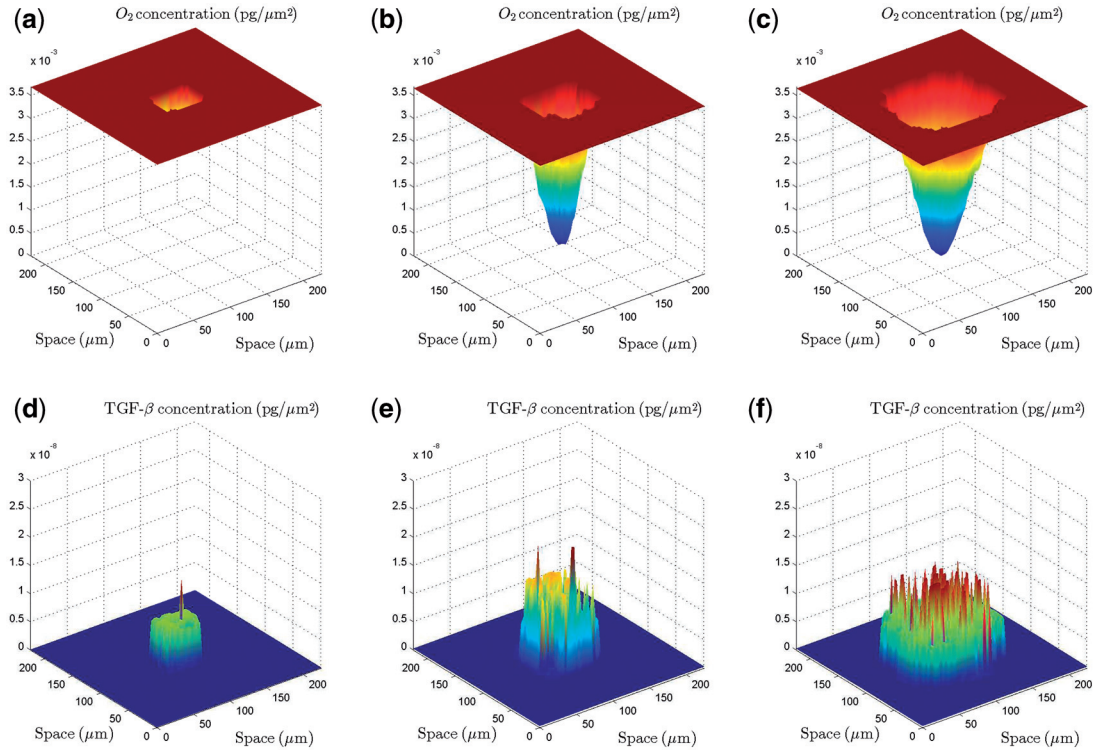

FIG. 6. Spatial distribution of the oxygen (a)–(c) and the TGF-β (d)–(f) in the case of 21% oxygen environmental concentration, at $t = 24, 48, 72$ h. Equations $(4.1)_{4,5}$ are solved in a domain $\Omega = [0, 225] \times [0, 225]$ (μm^2), with the model parameters given by Table 2.

5. Conclusions and perspectives

In this article, we developed a hybrid mathematical model describing the dynamics of cardiac biopsy-derived stem cells leading to the formation of the so-called Cardiosphere from a cluster of a few cells. The complexity of the problem is extremely high and the biological phenomena leading to the formation of a CSp are still not completely understood. Moreover, the quantitative characterization of the processes misses the estimate of some parameters essential for the accuracy of a mathematical model. Nevertheless, the proposed mathematical model appears in perfect agreement with the expected biological and pharmacological application shown in Messina *et al.* (2004); Chimenti *et al.* (2012, 2010); Forte *et al.* (2012). In particular, we were able to reproduce the basic structures of CSps assuming that only two elements are sufficient to describe the overall growth and maturation of the CSps: the oxygen as nutrient's emblem and the TGF-β as the chemical differentiation signal representative. Our choice to select these two key regulators of the CSps growth and differentiation gives us many more chances to easily foresee the main possible cellular consequences following experimental biological or pharmacological modifications, with a strong impact in both research quality and cost. The layered growth of the CSps, with a central proliferating region, surrounded by differentiated and less

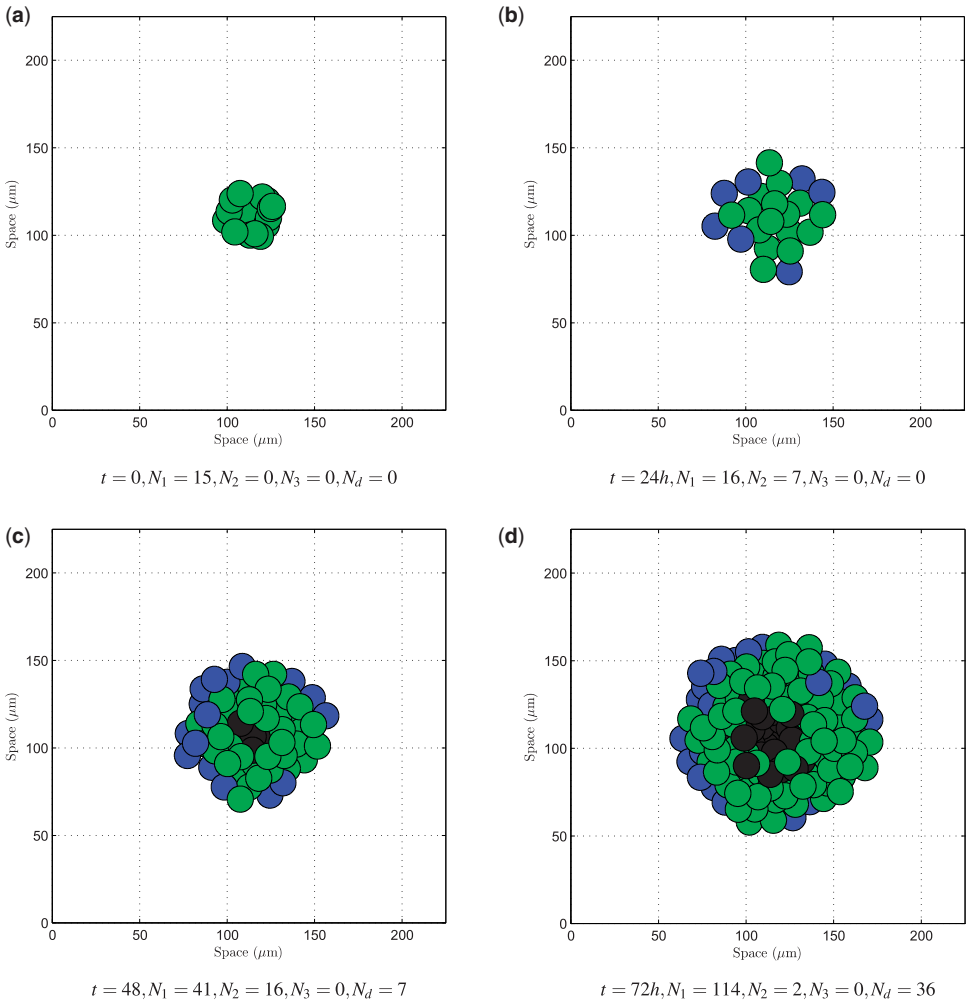

FIG. 7. (a)–(d) Numerical simulation of the CSp growth for a 5% oxygen environmental concentration, at times $t = 0, 24, 48, 72$ h. System (4.1) is solved in a domain $\Omega = [0, 225] \times [0, 225]$ (μm^2), with the model parameters given by Table 2. Differentiation levels are marked by different colours: green for the least differentiated cells ($\varphi = 1$), blue colour is for the intermediate level of differentiation ($\varphi = 2$), while the red colour labels cells with the highest degree of maturation ($\varphi = 3$). Black region indicates a necrotic/apoptotic core composed by dead cells. As in Fig. 5, N_1, N_2, N_3, N_d, in the subplot captions show the composition of the CSp at the displayed times. [Colour only in the online version.]

proliferating cells, has been observed in the numerical experiments. In this regards, the biological technology has a high potential for therapeutic purposes and possible strategies for further differentiated cells are under investigation (Lee *et al.*, 2013; Chen *et al.*, 2014). Furthermore, in a possibly more general framework, our modelling tool could be applied to many other cellular spheroid culture systems, such as tumour cells spheroids, induced-progenitor cells and embryoid bodies-derived stem cells.

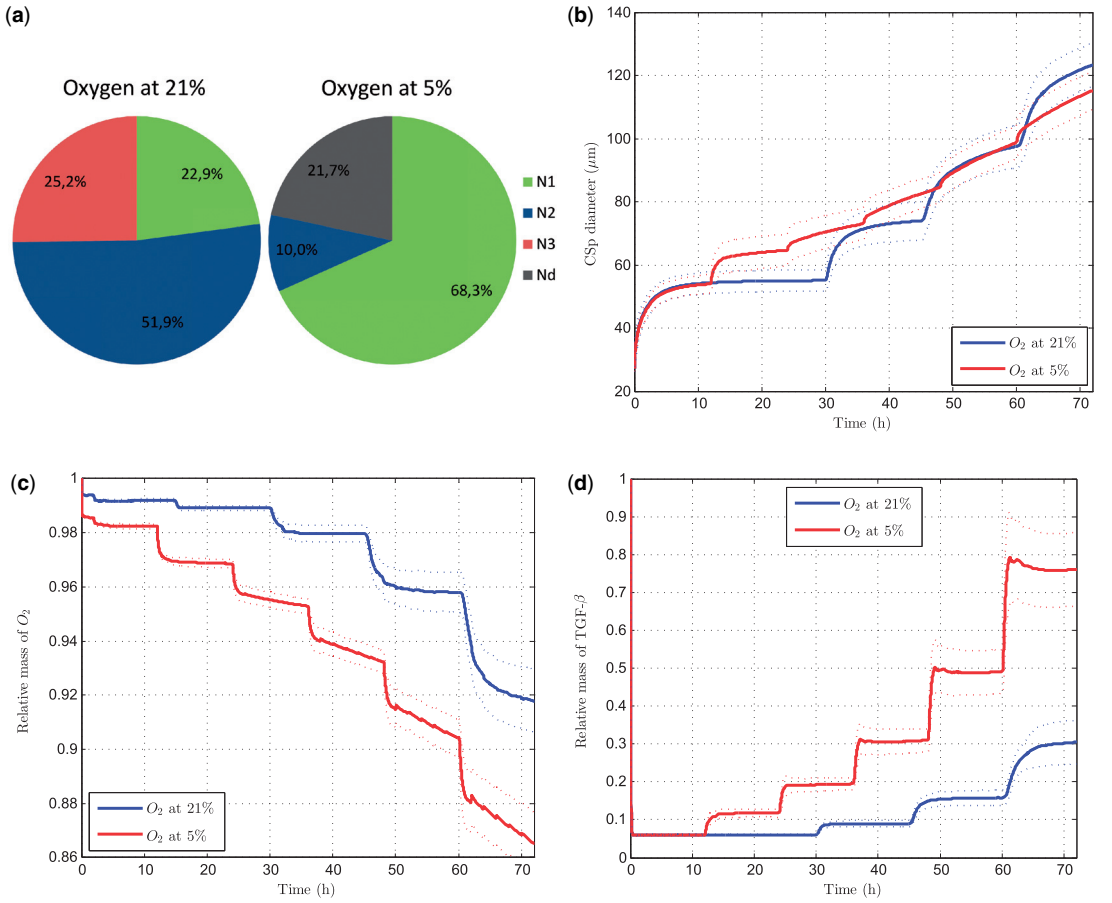

FIG. 8. (a) Pie charts describing the relative percentage distribution of the three types of cells (e.g. $(N_1/N_{\text{tot}}) * 100$) of a CSp in the case of 21% and 5% oxygen environmental concentration. The presented values are the averages over 100 independent simulations. (b) The diameter of the CSp as a function of time. (c) and (d) Oxygen and TGF-β relative masses, $m_{\text{rel}}(t) := m(t)/m(0)$ versus time. For all the figures, blue and red curves correspond respectively to 21% and 5% oxygen concentration. In figures (b)–(d), the solid line represents the average value computed over 100 simulations, while the dotted curves show the interval corresponding to one standard deviation. [Colour only in the online version.]

REFERENCES

AGATHOCLEOUS, M. & HARRIS, W. A. (2013) Metabolism in physiological cell proliferation and differentiation. *Trends Cell Biol.*, **23**, 484–492.

AIS PROJECT. (2001) Diffusion of molecules. *Web page*. URL: http://www.math.ubc.ca/~ais/website/status/diffuse.html. Department of Mathematics, University of British Columbia.

ANDERSON, A. R. A., CHAPLAIN, M. A. J. & REJNIAK, K. A. (eds) (2007) *Single-Cell-Based Models in Biology and Medicine*. Mathematics and Biosciences in Interaction. Basel, Switzerland: Birkhäuser.

ANDERSON, D. F., ERMENTROUT, B. & THOMAS, P. J. (2015) Stochastic representations of ion channel kinetics and exact stochastic simulation of neuronal dynamics. *J. Comput. Neurosci.*, **38**, 67–82.

BAYLY, P. V., TABER, L. A. & CARLSSON, A. E. (2012) Damped and persistent oscillations in a simple model of cell crawling. *J. R. Soc. Interface*, **9**, 1241–1253.

BELL, G. I., DEMBO, M. & BONGRAND, P. (1984) Cell adhesion. Competition between nonspecific repulsion and specific bonding. *Biophys. J.*, **45**, 1051–1064.

BROWN, G., HUGHES, P. J. & MICHELL, R. H. (2003) Cell differentiation and proliferation: simultaneous but independent? *Exp. Cell Res.*, **291**, 282–288.

CHAPLAIN, M. A. J. (2011) Multiscale mathematical modelling in biology and medicine. *IMA J. Appl. Math.*, **76**, 371–388.

CHEN, W.-P., LIU, Y.-H., HO, Y.-J. & WU, S. M. (2014) Pharmacological inhibition of tgf? Receptor improves nkx2.5 cardiomyoblast-mediated regeneration. *Cardiovasc. Res.*, **105**, 44–54.

CHIMENTI, I., GAETANI, R., BARILE, L., FORTE, E., IONTA, V., ANGELINI, F., FRATI, G., MESSINA, E. & GIACOMELLO, A. (2012) Isolation and expansion of adult cardiac stem/progenitor cells in the form of Cardiospheres from human cardiac biopsies and murine hearts. *Met. Mol. Biol.*, **879**, 327–338.

CHIMENTI, I., RUCKDESCHEL SMITH, R. & ET AL. (2010) Relative roles of direct regeneration versus paracrine effects of human cardiosphere-derived cells transplanted into infarcted mice. *Circ. Res.*, **106**, 971–980.

CLARELLI, F., DI RUSSO, C., NATALINI, R. & RIBOT, M. (2016) A fluid dynamics multidimensional model of biofilm growth: stability, influence of environment and sensitivity. *Math. Med. Biol*, **33**, 371–395.

DI COSTANZO, E. & NATALINI, R. (2015) A hybrid mathematical model of collective motion under alignment and chemotaxis. *Preprint*. URL: http://arxiv.org/abs/1507.02980. ArXive Repository.

DI COSTANZO, E., NATALINI, R. & PREZIOSI, L. (2015a) A hybrid mathematical model for self-organizing cell migration in the zebrafish lateral line. *J. Math. Biol.*, **71**, 171–214.

DI COSTANZO, E., NATALINI, R. & PREZIOSI, L. (2015b) A hybrid model of cell migration in zebrafish embryogenesis. *ITM Web Conf.*, **5**, 00013.

D'ORSOGNA, M. R., CHUANG, Y. L., BERTOZZI, A. L. & CHAYES, L. S. (2006) Self-propelled particles with soft-core interactions: patterns, stability, and collapse. *Phys. Rev. Lett.*, **96**, 104302–104305.

ENDERLING, H., HLATKY, L. & HAHNFELDT, P. (2012) The promoting role of a tumour–secreted chemorepellent in self-metastatic tumour progression. *Math. Med. Biol.*, **29**, 21–29.

FLETCHER, A. G., MURRAY, P. J. & MAINI, P. K. (2015) Multiscale modelling of intestinal crypt organization and carcinogenesis. *Math. Mod. Meth. Appl. S.*, **25**, 2563–2585.

FORTE, E., MIRALDI, F., CHIMENTI, I. & ET AL. (2012) TGFb-dependent epithelial-to-mesenchymal transition is required to generate cardiospheres from human adult heart biopsies. *Stem Cells Dev.*, **21**, 3081–3090.

FOURNIER, M. F., SAUSER, R., AMBROSI, D., MEISTER, J.-J. & VERKHOVSKY, A. B. (2010) Force transmission in migrating cells. *J. Cell Biol.*, **188**, 287–297.

ITOH, M. & CHITNIS, A. B. (2001) Expression of proneural and neurogenic genes in the zebrafish lateral line primordium correlates with selection of hair cell fate in neuromasts. *Mech. Develop.*, **102**, 263–266.

JOIE, J., LEI, Y., DURRIEU, M.-C., COLIN, T., POIGNARD, C. & SAUT, O. (2015) Migration and orientation of endothelial cells on micropatterned polymers: a simple model based on classical mechanics. *Discrete Continuous Dyn. Syst. Ser. B.*, **20**, 1059–1076.

KIM, Y. (2013) Regulation of cell proliferation and migration in glioblastoma: new therapeutic approach. *Front. Oncol.*, **3**, 1–17.

KUSHER, H. J. & DUPUIS, P. G. (1992) *Numerical Methods for Stochastic Control Problems in Continuous Time*. New York: Springer.

LEE, H.-J., CHO, H. J., KWON, Y. W., Y.-B., P. & KIM, H. S. (2013) Phenotypic modulation of human cardiospheres between stemness and paracrine activity, and implications for combined transplantation in cardiovascular regeneration. *Biomaterials*, **34**, 9819–9829.

LI, T.-S., CHENG, K., LEE, S. T. & ET AL (2010) Cardiospheres recapitulate a niche-like microenvironment rich in stemness and cell-matrix interactions, rationalizing their enhanced functional potency for myocardial repair. *Stem Cells*, **28**, 2088–2098.

MATSUDA, M. & CHITNIS, A. B. (2010) Atoh1a expression must be restricted by Notch signaling for effective morphogenesis of the posterior lateral line primordium in zebrafish. *Development*, **137**, 3477–3487.

MÉHES, E. & VICSEK, T. (2014) Collective motion of cells: from experiments to models. *Integr. Biol.*, **6**, 831–854.
MESSINA, E., DE ANGELIS, L., FRATI, G., MORRONE, S. & ET AL. (2004) Isolation and expansion of adult cardiac stem cells from human and murine heart. *Circ. Res.*, **95**, 911–921.
OSBORNE, J. M., WALTER, A., KERSHAW, S. K., MIRAMS, G. R., FLETCHER, A. G., PATHMANATHAN, P., GAVAGHAN, D., JENSEN, O. E., MAINI, P. K. & BYRNE, H. M. (2015) A hybrid approach to multi-scale modelling of cancer. *Phil. Trans. R. Soc. A.*, **368**, 5013–5028.
PREZIOSI, L. & TOSIN, A. (2009) Multiphase and multiscale trends in cancer modellings. *Math. Model. Nat. Phenom.*, **4**, 1–11.
RUBINSTEIN, B., FOURNIER, M. F., JACOBSON, K., VERKHOVSKY, A. B. & MOGILNER, A. (2009) Actin-myosin viscoelastic flow in the keratocyte lamellipod. *Biophys. J.*, **97**, 1853–1863.
RUCKDESCHEL SMITH, R., BARILE, L. & CHEOL CHO, H. E. A. (2007) Regenerative potential of Cardiosphere-derived cells expanded from percutaneous Endomyocardial biopsy specimens. *Circulation*, **115**, 896–908.
SALTELLI, A., RATTO, M., ANDREAS, T., CAMPOLONGO, F., CARIBONI, J., GATELLI, D., SAISANA, M. & TARANTOLA, S. (2008) *Global Sensitivity Analysis. The Primer*. Chichester: John Wiley & Sons, Ltd., 2008. xii+292 pp.
THERMO SCIENTIFIC (2007) Growth factors in thermo scientific hyclone cell culture serum. *Application Note* S0801. URL: https://static.thermoscientific.com/images/D22225∼.pdf. Thermo Fisher Scientific.
TSIMRING, L. S. (2014) Noise in biology. *Rep. Prog. Phys.*, **77**, 026601–026629.
VICSEK, T. & ZAFEIRIS, A. (2012) Collective motion. *Phys. Rep.*, **517**, 71–140.
WAKEFIELD, L. M., WINOKUR, T. S., S., H. R. & CHRISTOPHERSON, K. (1990) Recombinant latent transforming growth factor beta 1 has a longer plasma half-life in rats than active transforming growth factor beta 1, and a different tissue distribution. *J. Clin. Invest.*, **86**, 1976–1984.
WALLACE, D. I. & GUO, X. (2013) Properties of tumor spheroid growth exhibited by simple mathematical models. *Front. Oncol.*, **3**, 1–9.
WU, K., ROSTAMI, M. R. & ET AL. (2014) Oxygen transport and stem cell aggregation in stirred-suspension bioreactor cultures. *PLoS One*, **9** e102486. doi:10.1371/journal.pone.0102486.

Appendix Numerical scheme

Numerical simulations are obtained on a uniform Cartesian computational grid characterized by two positive parameters $\Delta x, \Delta y$. The nodes are $\mathbf{x}_{k,l} := (x_k, y_l) = (k\Delta x, l\Delta y)$, $k, l \in \mathbb{Z}$ and a generic finite volume cell is $C_{k,l} = (x_{k-1/2}, x_{k+1/2}) \times (y_{l-1/2}, y_{l+1/2})$. For a discrete time $t^m = m\Delta t$, $m \in \mathbb{N}$ the approximation of a function $f(t, x, y)$ is in standard notation $f^m_{k,l} = f(t^m, x_k, y_l)$ and $\mathbf{X}^m_i$, $\mathbf{V}^m_i$ denote the position and velocity respectively of the ith cell.
Now we present the elements of the numerical scheme used to approximate the mathematical model introduced in Section 3. In particular, we give details of the construction of the initial data for cells, we describe the approximation of the equations of motion for cells, of the reaction-diffusion equations for TGF-β and oxygen and the numerical code for the proliferation/differentiation processes. From now on we denote rand(a, b) a random number in the interval $[a, b]$ for any $a, b \in \mathbb{R}$.

- **Initial configuration of cells:** one cell is located at the centre of the domain and the rest $N^0 - 1$ cells are placed randomly around it with zero velocity

$$\mathbf{X}^0_1 = \left(\frac{L}{2}, \frac{L}{2}\right), \quad \mathbf{V}^0_1 = (0, 0),$$
$$r = \text{rand}(1.5R, 2R),$$
$$\theta = \text{rand}(0, 2\pi),$$
$$X^0_i = X^0_1 + r\cos\theta,$$

$$Y_i^0 = Y_1^0 + r\sin\theta,$$
$$\mathbf{V}_i^0 = (0,0).$$

- **Weighted average operator** $\mathcal{F}(h(\mathbf{X}_i,t))$, defined by (2.1), is approximated as follows

$$\mathcal{F}(h_i^m) \approx \frac{\sum_{\mathbf{x}_{k,l}\in B(\mathbf{X}_i^m,\bar{R})} w_i(\mathbf{x}_{k,l}) h_{k,l}^m}{\sum_{\mathbf{x}_{k,l}\in B(\mathbf{X}_i^m,\bar{R})} w_i(\mathbf{x}_{k,l})}.$$

- **Equations of motion.** The second order equation (3.1) is reduced to a system of first order equations. Then the position and the velocity of each cell i are approximated by the first order Euler method:

$$(1+\Delta t\mu)\mathbf{V}_i^{m+1} = \mathbf{V}_i^m + \Delta t\left(\sum_{\bar{i}\in I_i^m} \mathbf{K}(\mathbf{r}_{i,\bar{i}}) + \alpha\mathcal{F}(\nabla c|_{k,l}^m)\right)$$
$$\mathbf{X}_i^{m+1} = \mathbf{X}_i^m + \Delta t\mathbf{V}_i^{m+1},$$

where $I_i^m = \{\bar{i} : \mathbf{X}_{\bar{i}}^m \in B(\mathbf{X}_i^m, R_2)\backslash\mathbf{X}_i^m\}$. The gradient of the concentration of the TGF-β is approximated by the second order, centred difference

$$\nabla c|_{k,l} \approx \left[\frac{1}{2\Delta x}(c_{k+1,l} - c_{k-1,l}), \frac{1}{2\Delta y}(c_{k,l+1} - c_{k,l-1})\right].$$

- **Concentrations of chemical substances (TGF-β, Oxygen).** We apply the operator splitting algorithm between the space dimensions. The second order centred approximation of the Laplacian $\triangle f_{k,l}$ in each direction separately writes as

$$\partial_x(D(x,y)\partial_x f)|_{k,l} \approx \frac{1}{\Delta x}\left(D_{k+1/2,l}\partial_x f|_{k+1/2,l} - D_{k-1/2,l}\partial_x f|_{k-1/2,l}\right)$$
$$\approx \frac{1}{\Delta x^2}\left(D_{k+1/2,l}f_{k+1,l} - (D_{k+1/2,l} + D_{k-1/2,l})f_{k,l} + D_{k-1/2,l}f_{k-1,l}\right),$$

and analogically for $\partial_y(D(x,y)\partial_y f)|_{k,l}$.
Inside a cardiosphere, the diffusivity coefficients are of porous medium type. We denote

$$D_{k+1/2,l} = \frac{1}{2}(D_{k,l} + D_{k+1,l}), \text{ where } D_{k,l} = \frac{D^{\max}}{1+\rho\bar{A}_{k,l}}.$$

In order to compute the area of a finite volume $C_{k,l}$ occupied by cells we introduce in each $C_{k,l}$ the additional mesh grid $\Omega_{k,l}$ characterized by $\Delta\bar{x} << \Delta x$, $\Delta\bar{y} << \Delta y$. Computing the number $\mathcal{N}_{k,l}$ of nodes $\bar{x}_{p,q}$ such that

$$\bar{x}_{p,q} \in \Omega_{k,l} : \exists i = 1,...,N \quad \bar{x}_{p,q} \in B(\mathbf{X}_i, R),$$

we use the following approximation

$$\bar{A}_{k,l} = \mathcal{N}_{k,l}\frac{\Delta\bar{x}\Delta\bar{y}}{\Delta x\Delta y}.$$

The time integration of the reaction–diffusion systems is implicit for diffusion and stiff linear reaction terms, and explicit for other terms. More precisely, the update of the concentration of TGF-β is

$$S^*_{k,l} = S^m_{k,l} + \Delta t \triangle S^*_{k,l} + \Delta t \sum_{i=1}^{N} \xi_i \chi_{B(\mathbf{X}^m_i, R_3)},$$
$$S^{m+1}_{k,l} = S^*_{k,l} e^{-\Delta t \eta}.$$

For oxygen, the scheme writes as

$$c^{m+1}_{k,l} = c^m_{k,l} + \Delta t \triangle c^{m+1}_{k,l} - \Delta t \sum_{i=1}^{N} \frac{\lambda_i (c^m_{k,l})^{\gamma+1}}{k_i + (c^m_{k,l})^{\gamma+1}} \chi_{B(\mathbf{X}^m_i, R_3)} + \Delta t H \cdot (c_o - c^m_{k,l}) \bar{B}_{k,l},$$

where $\bar{B}_{k,l}$ is given by (3.13) with the mean radius of the sphere R_{CSp} approximated by

$$R_{\mathrm{CSp}} = \frac{1}{4} \left(\max_i X^m_i - \min_i X^m_i + \max_i Y^m_i - \min_i Y^m_i \right).$$

- **Proliferation and differentiation.** With each cell, we associate an internal timer $\varphi_i \to \bar{t}_i$. If $\bar{t}_i > T_c$ then a cell can proliferate or differentiate with some probability. After the proliferation and differentiation, the internal time is set to zero $\bar{t}_i \to 0$.
  At the numerical level, the order of appearance of the proliferation and differentiation has to be chosen. We assume that each occurs as first with the same probability. The following algorithm is used at each time step:

```
if rand(0,1)<0.5 then
  ⇒proliferation
    k = 1, for each i = 1,...,N
      if rand(0,1) < p_i
        r = rand(1.5R, 2R)
        θ = rand(0, 2π)
        X_{N+k} = X_i + r cos θ
        Y_{N+k} = Y_i + r sin θ
        V_{N+k} = V_i
        t_i = 0,  t_{N+k} = 0
        k → k + 1
      end
    end
  ⇒differentiation
    for each i = 1,...,N + k − 1
      if rand(0,1) < q_i/S_max and φ_i = 1,2
        φ_i → φ_i + 1
        t_i = 0
      end
    end
```

```
else
   ⇒differentiation
   ⇒proliferation
end
```

The proliferation threshold p_i is given by (3.9). Let us denote $\bar{c}_i = \mathcal{F}(c_i)$. The functions g are chosen as follows

$$g_1 = \begin{cases} 0, & \text{if } \bar{c}_i \le c_d, \\ g_1^{\max}\left[2\exp\left(-\ln 2\left(\dfrac{\bar{c}_i - c_1^{\text{opt}}}{c_d - c_1^{\text{opt}}}\right)^2\right) - 1\right], & \text{if } c_d < \bar{c}_i < c_1^{\text{opt}}, \\ g_1^{\max}\exp\left(-\left(\dfrac{\bar{c}_i - c_1^{\text{opt}}}{\delta_1}\right)^2\right), & \text{if } \bar{c}_i > c_1^{\text{opt}}, \end{cases}$$

$$g_{2,3} = \begin{cases} 0, & \text{if } \bar{c}_i \le c_d, \\ \dfrac{g_{2,3}^{\max}}{1-\epsilon_{2,3}}\left[\tanh\left(\delta_{2,3}\left(\bar{c}_i - c_{2,3}^{\text{opt}}\right)\right) - \epsilon_{2,3}\right], & \text{if } \bar{c}_i > c_d, \end{cases}$$

with $\epsilon_{2,3} = \tanh\left(\delta_{2,3}\left(c_d - c_{2,3}^{\text{opt}}\right)\right)$, c_d and $g_{1,2,3}^{\max}$ from Table 2, $c_1^{\text{opt}} = 9\times 10^{-4}$ pg μm^{-2} ($\approx 5\%$ oxygen), $c_{2,3}^{\text{opt}} = 2.5\times 10^{-3}$ pg μm^{-2} ($\approx 14\%$ oxygen), $\delta_1 = 5\times 10^{-4}$ pg μm^{-2}, $\delta_{2,3} = 2\cdot 10^3$ pg^{-1} μm^2. The differentiation threshold q_i is computed according to (3.3).